JETIR.ORG ISSN: 2349-5162 | ESTD Year : 2014 | Monthly Issue
JOURNAL OF EMERGING TECHNOLOGIES AND INNOVATIVE RESEARCH (JETIR)
An International Scholarly Open Access, Peer-reviewed, Refereed Journal

PSEUDO CT GENERATION FOR THE DETECTION OF BONE LESIONS BASED ON HYBRID DCNN-GAN

[1]Sreeja.S
[1]Assistant Professor
[1]Department of Computer Science
[1]Government College Kariavattom, Thiruvananthapuram , India

Abstract : Nowadays, medical imaging has an important role in radiotherapy and treatment planning process. Despite the increasing usage of the magnetic resonance imaging (MRI) in the external radiotherapy (RT) design process. MRI is only radiotherapy treatment planning is attractive since MRI provides superior soft tissue contrast without ionizing radiation compared with computed tomography (CT). CT-scans are the main imaging modality in external beam radiotherapy. They allow the definition of tissue electron density necessary for dose calculation. A magnetic resonance (MR)-only radiotherapy workflow can reduce cost, radiation exposure and uncertainties. However, it requires the generation of pseudo CT from MRI images for patient setup and dose calculation. A crucial prerequisite is generating the so called pseudo-CT (pCT) images for accurate dose calculation and planning. Our proposed GAN (Generative Adversarial Network) method to generate pseudo CT images has been shown to provide pseudo CT images with excellent image quality. In this study, the main aim is to allow pseudo-CT images to be generated from MRI data for the diagnosis of bone lesions and investigate the accuracy of dose calculation in brain frameless Stereotactic Radio Surgery (SRS) using pseudo CT images which are generated from MRI images using the Deep Convolutional Neural network method. The outcome of a detailed assessment of various strategies for GAN, brain bone lesion identification from magnetic resonance imaging (MRI) was exploited to select the optimal parameters and setting, with the aim of proposing a DCNN based GAN pseudo-CT generation approach.

IndexTerms **- Computed Tomography (CT),GAN (Generative Adversarial Network) (pCT),Radiotherapy (RT).**

1. INTRODUCTION

Whole-body examination is still challenging in CT/PET/MR scanners. The evolution of CT, PET and MRI into complementary in vivo molecular imaging techniques has generated increased interest in the development of combined PET/MRI systems. However, many challenges have slowed the adoption of the recently developed simultaneous PET/MR scanners. MRI is used to diagnose, plan therapy, and monitor the progression of a variety of neurological illnesses, including brain tumors [1]. Alzheimer's disease [2], Parkinson's disease [3], multiple sclerosis [4], stroke [5] and other neurodegenerative illnesses are examples of neurodegenerative disorders. Computed tomography (CT) plays a significant role in treatment planning and dose calculation in the radiation therapy (RT) chain by providing 3-dimensional attenuation coefficient maps. These are used to calculate organ and tissue-specific doses (1). Modern techniques, such as intensity modulated radiation therapy (IMRT) and volumetric-modulated radiation therapy (VMAT), rely on anatomical images to accurately define the target and organs at risk (OAR) for proper dose delivery. In clinical practice, the use of magnetic resonance imaging (MRI) for treatment planning is increasing due to the high contrast soft-tissue discrimination and sharper organ boundaries possible in comparison with CT imaging. MRI is clearly superior to CT for organ delineation and could therefore improve tumor targeting in dose planning. However, MRI does not provide electron density information that is necessary for dose calculation [6]. To overcome this issue, several methods have been developed to generate pseudo-CTs (pCTs) for MRI-based dose planning.

Machine learning approaches have previously been proposed to estimate attenuation maps. A few pilot studies utilizing neural network methods have shown promising results in PET/MR imaging. These studies typically rely on the inputs of T1-weighted MR images, ultrashort-echo time MR images and transmission images to estimate pseudo-CTs which can be applied to PET attenuation correction [7]. More recently, deep learning approaches using Convolutional Neural Networks (CNN) have been applied to medical imaging with successful implementations across a diverse range of applications [8]. Deep learning methods are more advanced forms of neural networks and utilizing many levels of network structures capable of learning image features by a series of image convolution processes. One recent study used deep learning to generate discrete pseudo-CTs for MR attenuation correction using a single T1-weighted head image, which significantly reduced error in an evaluation dataset of brain images [9, 10]. The brain is difficult to separate into different tissue classes because the strength levels of bone and air signals are so near. As a consequence, the study's main contribution is to overcome the problem of attenuation correction in bone lesion identification by creating pseudo-CT images from MR Images. This was accomplished using the pre-processing component of the image

registration procedure. Finally, the GAN model has been newly adapted for pseudo-CT generation, which produces the most similar bone regions as shown in CT images.

2. LITERATURE SURVEY

A comprehensive review of PCT for PET/MRI can be found at [11-21]. Briefly, current methods for attenuation correction in PET/MRI can be grouped into the following categories: Some studies have shown that functional MRI information, including diffusion-weighted imaging (DWI) and dynamic contrast enhanced imaging, could aid in identifying active tumor sub-volumes in head and neck cancer. Korsholm et al., [11] has suggested that a 2% error in MRI dose calculation is clinically acceptable. In addition, with this technique, it is difficult to create reference images that could be used for patient positioning verification due to the lack of bone segmentation. An alternative methodology is to separate the tissues in the MR image into different classes and assign every class an electron density or Hounsfield unit (HU) value. In most cases this involves two or three classifications; soft tissue and bone (and in some cases air). Improved dosimetric results have been reported using these techniques compared to using a homogeneous density override, namely for prostate, brain and head and neck site. Stanescu et al., [12] attempted a semi-automatic method of bone segmentation in the head. Here, a point was placed close to the structure which required segmentation. Thresholding was then used to segment the structure. The authors noted that manual adjustment afterwards was required in some cases, particularly towards the lower section of the skull. Paula et al., [13] used an atlas-based segmentation method to separate the bone, prior to bulk density override. Again manual adjustment was used if necessary. Methods such as these could mean that bulk density techniques are more useful in a clinical workflow in the future, although manual adjustment of contours would not be desirable.

Atlas-based techniques typically use a single, standard MRI sequence in order to produce an sCT. This ensures that scanning time is kept to a minimum, reducing the chances of patient movement. It also means that the scanning protocol is straightforward to implement in a clinical environment. The process for sCT production can be fully automated and reference images for positioning verification can be produced as well as automatic contouring of OARs. Sjolund et al., [14] remarked how atlas-based techniques are relatively robust to image artifacts due to their reliance on prior training information. The simplest atlas techniques use a single or average atlas, for example as developed by Dowling et al.[15], for prostate planning. With an average atlas technique, pairs of MRI and CT scans from a database of patients are co-registered. An average MRI atlas is then created, potentially with a matching set of organ contours. By determining the deformations which need to be applied to each MRI scan in the database to reach the average atlas, an average CT atlas can be created by applying the same deformations to the corresponding registered CTs and finding the average of these. In order to create an sCT for an incoming MR image, the average MRI atlas is registered to the incoming MRI scan. These deformations are then applied to the average CT atlas resulting in a corresponding sCT. The organ contours can be propagated similarly.

CBCT-to-CT conversion via DL is the most recent CT synthesis application. For what concerns the latest development from the deep learning perspective, in 2018, Oktay et al.[16] proposed a new mechanism, called attention gate (AG), to focus on target structures that can vary in shape and size. Liu et al.[17] incorporated the AG in the generator of a cycle-GAN to learn organ variation from CBCT-CT pairs in the context of pancreas adaptive RT, showing that its contribution significantly improved the prediction compared to the same network without AG. Alternatively, it would be quite interesting if a CNN could automatically generate a metric to assess the quality of sCTs, as, Matt et al.[18] proposed using uncertainty for such a task adopting a multi-task network and a Bayesian probabilistic framework. More recently, two other works proposed to use uncertainty either from the combination of independently trained networks or via dropout-based variational inference. So far, the field of uncertainty estimation with deep learning has been just superficially touched for sCT generation. It would be interesting to see future work focusing on developing criteria for the automatic identification of failure cases using uncertainty prediction. Patients with inaccurate synthetic CTs will be agged for CT rescan, or manual adjustment of the sCT if deemed feasible.

Andrew et al. [19] proposed a Bayesian deep convolutional neural network, in addition to generating an initial pseudo-CT from MR data, also produces uncertainty estimates of the pseudo-CT to quantify the limitations of the MR data. Angel et al. [20] proposed a network that maps between the four 2-dimensional (2D) Dixon MR images (water, fat, in-phase, and out-of-phase) and their corresponding 2D CT image. Author assessed the accuracy of the μ-maps and reconstructed PET images by performing voxel- and region-based analysis comparing the SUVs (in g/mL) obtained after AC using the Dixon-VIBE (PETDixon), DIVIDE (PETDIVIDE), and CT-based (PETCT) methods Axcel et al. [21] evaluated and compared the U-Net and GAN DLMs using various hyperparameters and loss functions (L_2, single-scale PL, multiscale PL, weighted multiscale PL) as well as PBM, for prostate cancer MRI-only dose planning. By analyzing the above-mentioned works of literature on pseudo-CT generation from magnetic resonance images, the author was motivated to develop a technique for accurately extracting the bone lesion from magnetic resonance images.

Objectives:

- This study aims to improve patient positioning and dose targeting in brain MRI-only radiotherapy by using MRI acquired in treatment position.
- The main goal of this study was to investigate the possibility of removing the CT simulator from the brain MRI and replacing it with synthetic-CT images and calculating the electron density values for designing patient treatment planning.
- In this work proposed a novel ***deep convolutional neural network with GAN (DCNN-GAN)*** method for pCT generation and evaluate the bone lesions on a set of brain tumor patient images
- It is investigated whether there is a relationship between MRI intensity and CT- HU value within different regions.
- The purpose is to find a simple and efficient model that could provide electron density information from the MRI images to generate the Pseudo CT images with an acceptable error rate that could be used in clinical RT treatment planning.

The remainder of this questionnaire is arranged as follows. Section 2 presents the main deep learning techniques that have been used for Image generations are described in the survey. In image generation, Section 3 describes the methodology of DCNN-GAN to the generation of pCT: enhancement, detection. In various areas of use, Section 4 analyses the findings obtained and the open challenges. Finally the work is concluded in section 5.

3. METHODOLOGY

Figure 1 depict the overall structure of the proposed system in which initially data are collected from the popular dataset i.e., RIRE. From these raw data, there can be a chance of noises and other anomalies which are needed to be pre-processed for further processes in which techniques used are outlier elimination, data smoothening and normalization. Once these are pre-processed, then generate pCT, using DCNN-GAN.

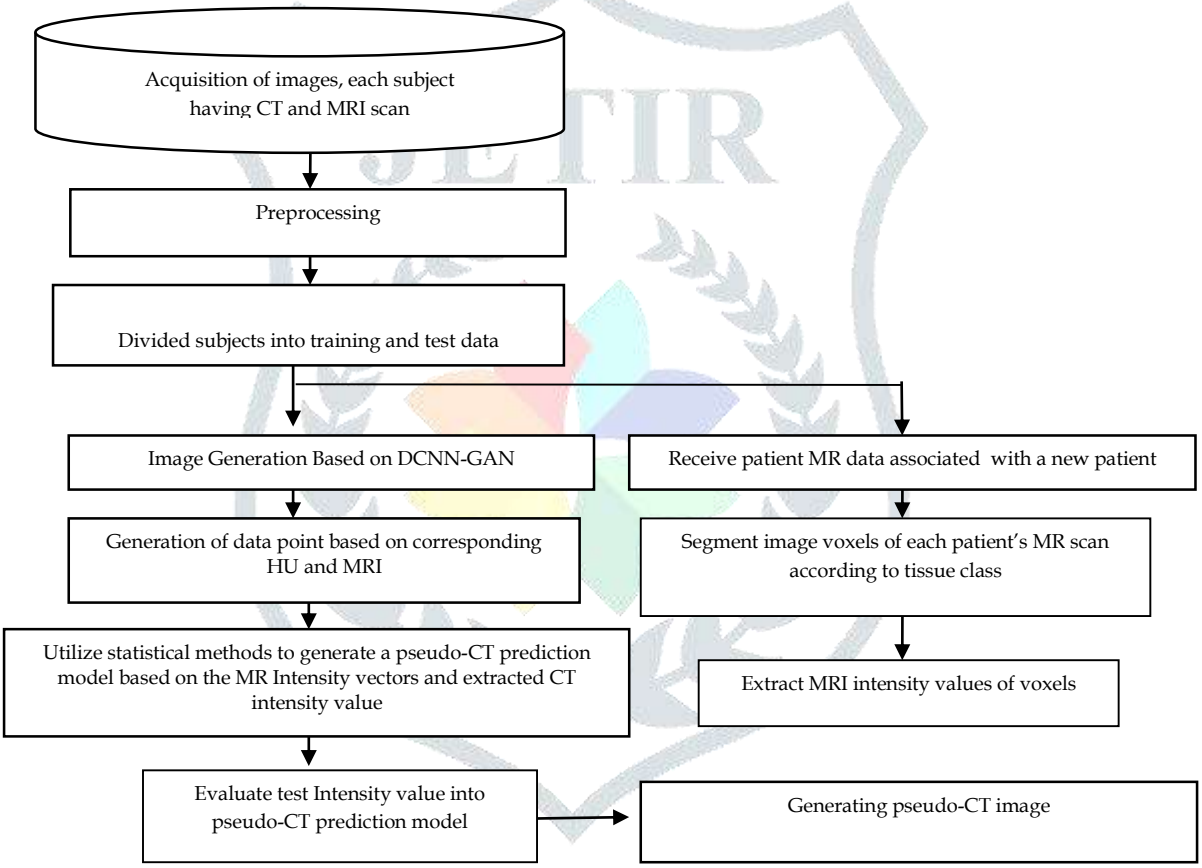

Figure 1: proposed block diagram

1.1. Image Acquisition

While certain files, such as OASIS and the Alzheimer's Neuro imaging Initiative [22] have the same MRI data and CT data, public databases containing both modalities for the same person are unusual. To our knowledge, MRI and CT image from the same subject are only found in the RIRE project and the Cancer Imaging Archive. Because the RIRE project uses a common data format, we employed it for our investigation. The RIRE dataset's aggregated modality count is given in the first row of Table 1.

Table 1. Subject counts of RIRE with respect to image modalities

CT	MRI PD	MRI T1	MRI T2	MRI MP RAGE	PET
17	14	19	18	9	8

In rare cases, positron emission tomography (PET) can be acquired in addition to CT images for select individuals. A corrected version of certain MRIs is available, but we didn't utilize it. Because they provided the most participants, T1 weighted MRI and CT were chosen as input and goal data. However, supplying different MRIs as multi-channel input would be a fascinating experiment.

1.2. Pre-processing of MRI and CT images:

Today's real-world databases are highly susceptible to noisy, missing, and inconsistent data due to their typically huge size (often several gigabytes or more) and their likely origin from multiple, heterogenous sources. Low-quality data will lead to low-quality mining results. There are a number of data preprocessing techniques [23]. In this work outlier elimination, data smoothening and

normalization methods are proposed to enhance the input images. These techniques are not mutually exclusive; they will work together.

- **Outlier elimination:** Outliers are data points that deviate away from the general trend of the dataset. These outliers affect the performance of the system as they seem to be inconsistent with the dataset. They tend to shift the mean and scatter of the data away from their ideal values, which affects the performance of the proposed system [24]. The removal of outlying observations helps in improving the quality of training. Outlier removal essentially reduces noise in the dataset, which might occur due to mechanical faults, changes in system behavior, human error, instrument error, etc. The commonly used outlier elimination methods are the block D/R and Tukey elimination procedures. The block D/R procedure eliminates values based on the D/R ratio. the Tukey method eliminates all values more than 1.5 IQRs away from the first and third quartiles (Inter Quartile Range).
- **Data smoothening:** Data smoothening provides methods to deal with dirty data. Since dirty datasets can cause problems for data exploration and analysis, data smoothening techniques have been developed to clean data by filling in missing values (value imputation), smoothing noisy data, identifying and/or removing outliers, and resolving inconsistencies. Noise is a random error or variability in a measured feature, and several methods can be applied to remove it. Data can also be smoothed by using regression to find a mathematical equation to fit the data [25]. Smoothing methods that involve discretization are also methods of data reduction since they reduce the number of distinct values per attribute. Clustering methods can also be used to remove noise by detecting outliers.
- **Data normalization:** Data transformations, such as normalization, may be applied, where data are scaled to fall within a smaller range like 0.0 to 1.0. This can improve the accuracy and efficiency of mining algorithms involving distance measurements. Many data mining algorithms provide better results if the data has been normalized or scaled to a specific range before these algorithms are applied [26]. The use of normalization techniques is crucial when distance-based algorithms are applied, because the distance measurements taken on by attributes that assume many values will generally outweigh distance measurements taken by attributes that assume fewer values. Other methods of data normalization include data aggregation and generalization techniques. These methods create new attributes from existing information by applying summary operations to data or by replacing raw data by higher level concepts.

1.3. DCNN based GAN method

Here hybrid models are used for pCT , such as DCNN based GAN. CNN is one of the techniques used for the pCT generation purpose. However the CNN model requires large amount of dataset to avoid this GAN model is used. GAN models main purpose is to reduce the dataset; this model will automatically select the features that accompany this generation. This method adjusting the parameters such as weights and learning rates to reduce the loss. The CNN (convolutional neural Network) is an artificial neural network that KunihikoFukushima[27] and Yann LeCan et al . introduced in 1980[28][29]. CNN consists of 6 layer types: input layer, wrapping layer, nonlinear layer, pool layer, output layer and completely connected layer.

A collection of convolutional nuclei in which each neuron behaves as a nucleus is made up of the convolutional layer. However, if the kernel is symmetrical, the convolution operation becomes a correlation operation (Ian Good fellow et al., 2017). The convolutional kernel works by slicing the picture into small slices, commonly known as receptive fields. You may express the convolution operation as follows:

$$t_1^k(p,q) = \sum_c \blacksquare \blacksquare \sum_{x,y} \blacksquare \blacksquare i_c(x,y).e_1^k(u,v) \qquad (1)$$

Where, $i_c(x,y)$is an element of the input image tensor I_c , which is element wise multiplied by $e_1^k(u,v)$ index of the k[th] convolutional kernel k_1 of the l[th] layer. Whereas output feature-map of the k[th] convolutional operation can be expressed as $F_1^k = [t_1^k(1,1),...(t_1^k(p,q),..t_1^k(P,Q))]$.

When properties are maintained in the pool layer, their precise location becomes less important as long as their approximate position relative to others is maintained. An interesting local activity is pooling, or down sampling. It aggregates similar data in the receiving field neighbourhood and generates the dominant response within that local area.

$$Z_l^k = g_p(F_l^k) \qquad (2)$$

Equation (2) shows the pooling operation in which Z_l^k represents the pooled feature-map of l[th] layer for k[th] input feature-map F_l^k , whereas $g_p(.)$defines the type of pooling operation.The use of the pooling operation allows to extract a mix of features that are invariant to minor distortions and translational changes. In equation (10), the activation function for a convoluted feature-map is described.

$$T_l^k = g_a(F_l^k) \qquad (3)$$

the above equation, $F_l^k$is an output of a convolution, which is assigned to activation function $g_a(.)$That adds non-linearity and returns a transformed output $T_l^k$for lth layer.

Batch normalisation is used within feature-maps to resolve the problems associated with the internal covariance change. The internal covariance shift, which slows down convergence (by moving the learning rate to a small value) and requires careful parameter initialization, is a change in the distribution of hidden unit values.Batch normalization for a transformed feature-map $F_l^k$is shown in equation (4).

$$N_l^k = \frac{F_l^k - \mu_B}{\sqrt{\sigma_B^2 + \varepsilon}} \qquad (4)$$

In equation (4), N_l^k represents normalized depict mean andμ_B and σ_B^2feature-map, F_l^k is the feature-map input, B variance of a feature-map for a mini batch. Inside the network, Dropout introduces regularisation, which gradually enhances generalisation by

randomly omitting certain units or links with a certain probability. At the end of the network, the completely connected layer is mainly used for classification.

It is a global process, but it requires large amount of data for generating better results. Likewise the primary objective in deep learning is to have a network that performs its best on both training data & the test data/new data it hasn't seen before. Adopting such imbalanced data will make the model less sensitive to samples with higher DR severity levels and lead to overfitting. Although common data augmentation methods such as flipping and random cropping and rotation can mitigate the problem, the poor diversity of samples from those levels still limits model performance. To solve this problem GAN architecture is used. If the training data is insufficient GAN can automatically train based on the input datasets and generate the synthesis images, this will augment the input dataset.

GAN: Recent ideas based on Generative Adversarial Networks (GANs) [30] are able to overcome this problem by learning a more suitable loss function directly from data [31]. The basic block of GAN architecture is shown n figure 2. Generative Adversarial Networks (GAN) have achieved state-of-the-art results in the field of image generation producing very realistic images in an unsupervised setting The underlying strategy of adversarial methods consists of emulating a competition, in which the mapping G, called Generator, attempts to produce realistic images, while a second player, the Discriminator D, is trained to distinguish the output generated by G from real examples.

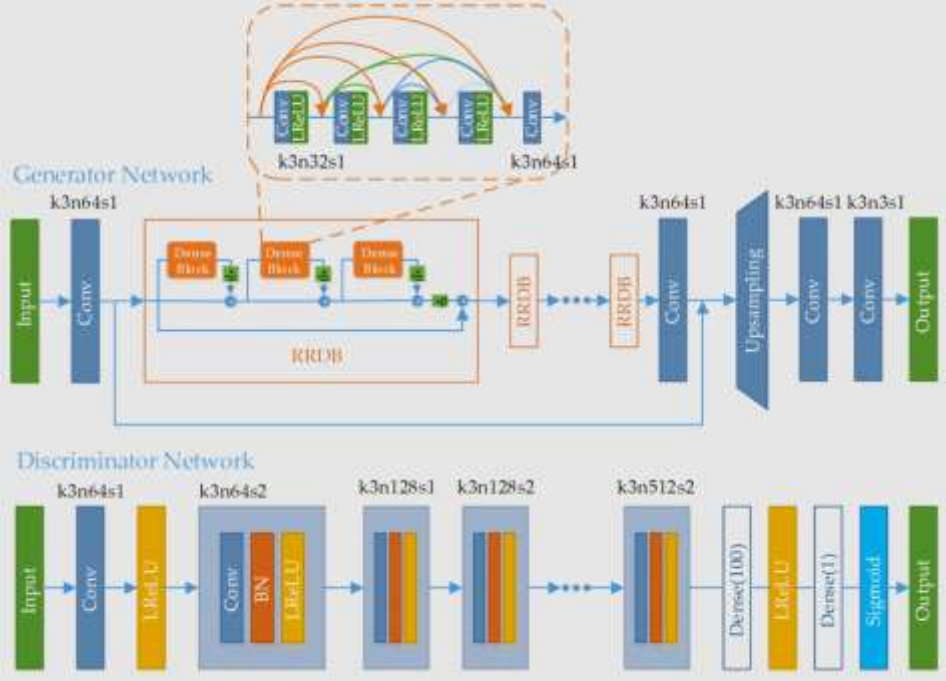

Figure 2: Basic blocks of GAN architecture

Here, both G and D are neural networks, and act as adversaries, since the goal of G is to maximize the misclassification error of D, while D's objective is to beat G by learning to identify generated images. As in (4), the adversarial loss, driving the learning of G and D, is:

$$L_{adv}(G,D)=E_{v,r\sim p_{data(v,r)}}\left[log\,log\left(D(v,r)\right)\right]+E_{v,r\sim p_{data}}(v)\left[log\,log\left(1-D(v,G(v))\right)\right] \quad (5)$$

Where $E_{v,r\sim p_{data}}(v,r)$ is the expectation over the pairs (v,r), sampled from the joint data distribution of real pairs $p_{data(v,r)}$ and $p_{data(v)}$ is the real vessel trees distribution. The Discriminator's objective is to maximize (1), while the Generator's goal is to minimize it. Therefore, it is D that provides the training signal to G, replacing more conventional loss functions.

Although minimizing the above loss function induces G to produce visually sharp results, recent work in [12], [14] has shown that combining Eq. (5) with a global L_1 loss provides more consistent results. Thus, the loss function to optimize becomes:

$$L_{im2im}(G,D)=L_{adv}(G,D)+\lambda E_{v,r\sim p_{data(v,r)}}[\|r-G(v)\|_1] \quad (6)$$

where λ balances the contribution of the two losses. The discriminator's objective is in this case local, i.e., it attempts to discriminate $N\times N$ image regions as real or generated, but the goal of G is supplemented with a requirement not only to generate realistically looking images but also images that preserve a global regularity. Since the L_1 loss guarantees that the output of G is globally consistent, D can concentrate.

The optimization process consists of two alternate stages. In the first step, the discriminator is updated to distinguish samples generated by q from those coming from the prior distribution p(z). This is achieved by maximizing the following loss:

$$L_{code}(D_{code},q)=E_{z\sim P(z)}\left[log\,log\left(D_{code}(z)\right)\right]+E_{v,r\sim p_{data}(v)}[log(1-D_{code}(q(\tfrac{z}{v})))] \quad (7)$$

In addition, both the encoder and the decoder weights are updated to minimize the reconstruction error and, at the same time, to maximize the classification error of the discriminator. In this way, the complete loss function that drives the learning of the adversarial auto encoder is a combination of both losses:

$$L_{AAE}(D_{code},q,p)=L_{code}(D_{code},q)+\gamma L_{rec}(q,p) \quad (8)$$

Where, γ weights the importance of the two losses. The goal of q and p is to minimize L_{AAE}, while D_{code} attempts to maximize it. When the optimization process reaches an equilibrium point of Eq. (8), the decoder p defines a generative model than can be employed to generate new vessel trees starting from a sample of the imposed prior p(z) on the latent distribution. In our case, the loss functions defining both models are differentiable almost everywhere. Accordingly, to build a joint loss function we can directly combine them by simple addition. Nonetheless, we need to redefine the image to- image losses in Eqs. (6) and (7), so that they take the output of the adversarial auto encoder as the input to G:

$$\tilde{L}_{adv}(G,D)=E_{v,r\sim p_{data(v,r)}}[log\,log\,(D(v,r))]+E_{v,r\sim p_{data}}(v)[log\,log\,(1-D(\tilde{v},G(\tilde{v})))] \quad (9)$$

$$\tilde{L}_{im2im}(G,D)=\tilde{L}_{adv}(G,D)+\lambda E_{v,r\sim p_{data(v,r)}}[\|r-G(\tilde{v})\|_1] \quad (10)$$

where $\tilde{v}=p(q(v))$ is the vessel tree generated by the adversarial autoencoder. With this modification, both loss functions can be linearly combined into a global one:

$$L(G,D,D_{code},q,p)=\tilde{L}_{im2im}(G,D)+L_{AAE}(D_{code},q,p) \quad (11)$$

In this formulation, the goal of G, q and p is to minimize the loss function in Eq. (11), while D and D_{code} attempt to maximize it. The main advantage of this joint training scheme is that the discriminator D also provides with a better loss function for the adversarial auto encoder. The decoder p needs to produce realistic looking vessels in order to maximize the misclassification of D. Also, part of the training signal that arrives to p flows through G. As a consequence, the adversarial auto-encoder also benefits when the generator produces realistic pCT images.

Evaluation Metrics:

The voxel-wise Mean Absolute Error (MAE) and the Mean Error (ME) are the most fundamental and extensively used measuring scales for evaluating the quality of a pseudo-CT image:

$$MAE_{vox}=\frac{1}{N_C}\sum_{n=1}^{N_C}\blacksquare\,|CT(n)-pCT(n)| \quad (12)$$

$$ME_{vox}=\frac{1}{N_C}\sum_{n=1}^{N_C}\blacksquare\,CT(n)-pCT(n) \quad (13)$$

$$SSIM=\frac{(2\mu_x\mu_y+l_1)\,(2\sigma_{xy})l_2)}{(\mu_x^2+\mu_y^2+l_1)\,(\sigma_x^2+\sigma_y^2+l_2)} \quad (14)$$

$$DC=\frac{2\times TP}{(TP+FP)+(FN+TN)} \quad (15)$$

$$Accuracy=\frac{TP+TN}{TP+FP+FN+TN}\times 100\% \quad (16)$$

4. RESULTS AND DISCUSSION:

The model was created using Windows 10 and MATLAB for simulation. For a single pCT from MRI, one epoch of neural network training takes 50 iterations to run through all of the training data once, resulting in a computation time of 37 seconds. The Mean Absolute Error (MAE) and Mean Error (ME) values for the total body were calculated to accomplish this. The RIRE dataset was utilized to create pseudo-CT investigations, as previously stated.

The output image derived from the DCNN-GAN model is depicted in Figure 3 as a pseudo-CT generation, in which the bone lesions are successfully predicted from the input MRI image. The best accurate identification of bone lesion was achieved by performing absolute image registration with DCNN and feature extraction up to GAN features. Here table 2 & figure 4 shows the computational time of the proposed work.

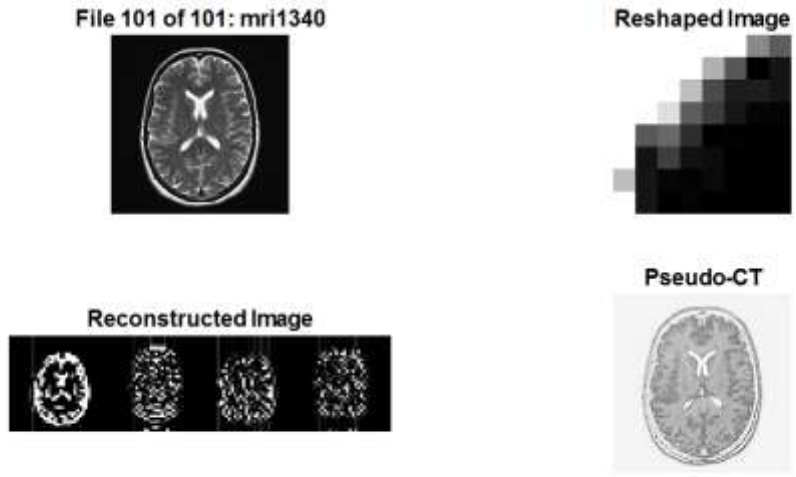

Figure 3: GAN output as generated pseudo-CT image

Table 2. Comparison of computation time

Models	VGG16	Resnet	Alexnet	Densenet	CNN	DCNN-GAN
Time	5.78	8.93	8.89	7.02	5.50	4.21

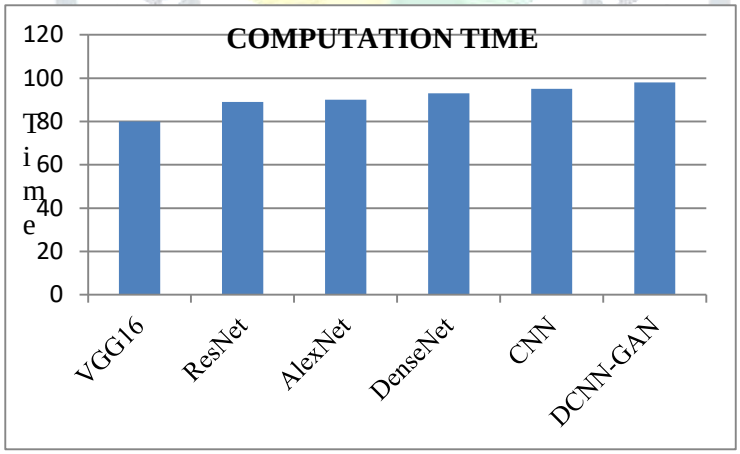

Figure 4: CT vs Models

Table 3. Comparison of SSIM similarity measure

Measure	VGG16	Resnet	Alexnet	Densenet	CNN	DCNN-GAN
DC	0.79±0.03	0.83±0.02	0.86±0.01	0.92±0.02	0.90±0.04	0.94±0.02
SSIM	0.84±0.03	0.86±0.03	0.84±0.04	0.89±0.02	0.87±0.04	0.86±0.05

Table 3 & Figure 5 represents the comparison of SSIM and DC similarity measures between the original CT and the resulting pseudo-CT images. From the figure 6 and table 4, it is understood that the GAN can obtain 86% of similarity to the original CT image and 94% of DC. The mean square error obtained by the proposed GAN based pseudo-CT generation for bone lesion detection has been depicted in figure 6. The mean absolute error is obtained as 10.1053 at the training phase and 9.72 at the testing phase.

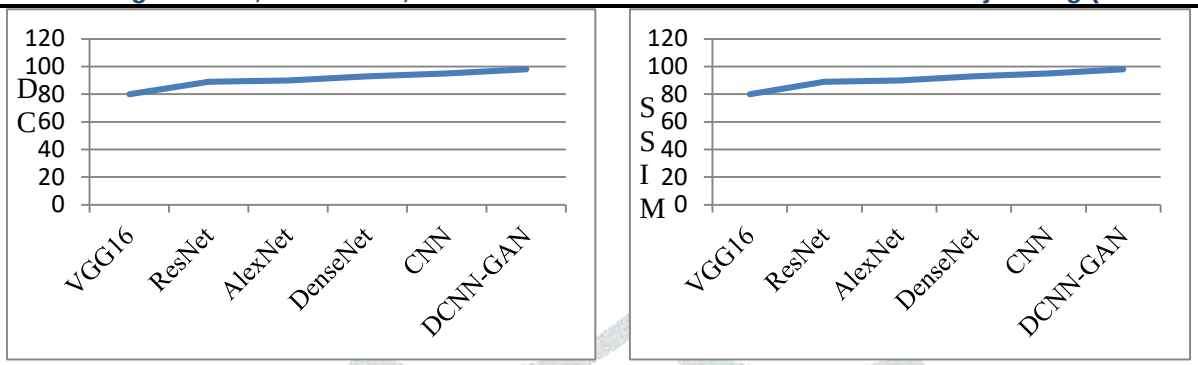

Figure 5: a) DC vs Models b) SSIM vs Models

Table 4. Comparative analysis of various models under MAE, MSE

Measure	VGG16	Resnet	Alexnet	Densenet	CNN	DCNN-GAN
MAE (HU)	72.3±1.18	64±10.12	76.8±9.30	84±3.90	82.3±2.34	67.5±17.3
MSE (HU)	100.3±44.2	118.2±20.9	167±18.5	233.1±12.2	188±27.7	188±33.7

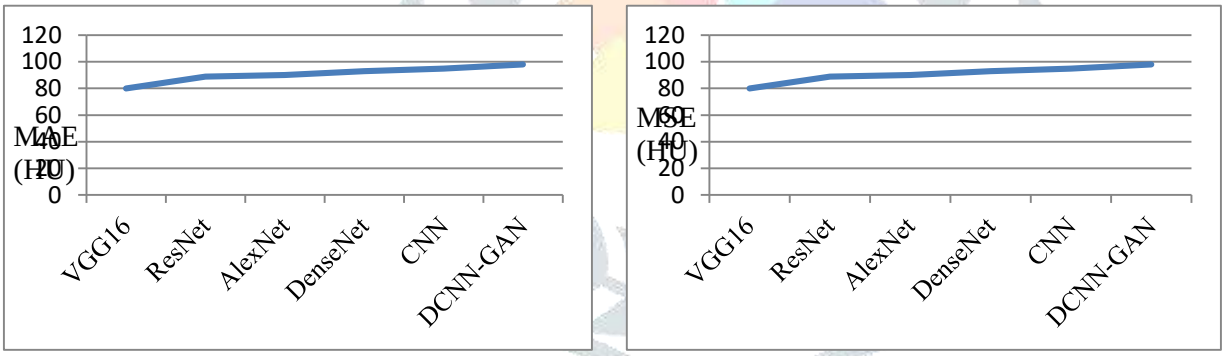

Figure 6 a) MAE vs Models b) MSE vs Models

Figure 6 (a, b) depict the graphical representation of various models evaluated under MAE and MSE. Figure 7 (a) depicts the graphical representation of the accuracy. The proposed work obtains 98% accuracy compared to other models.

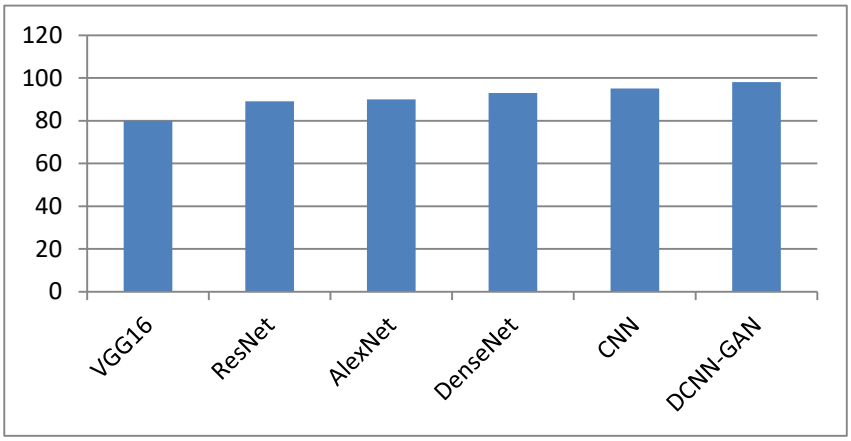

Figure 7 a. Classification model vs Accuracy

The proposed work of the generation of pCT from MRI for effective bone tumour analysis, mostly this will be potentially helpful for the healthcare community (neurosurgeons) and research community for better integration and development of a model for even more accurate results from theoretical and practical aspects.

CONCLUSIONS

Computer Tomography remains a basic imaging modality in radiotherapy because of its relation with electron density value. In conventional external radiotherapy, MRI is used in functional tissue structures with registration on the CT image, which causes systematic errors during the registration of MRI and CT image. Generally, diagnosis of brain disorders requires correct diagnosis. Any misdiagnosis results in damages that are irreparable. The occurrence of bone lesions in patients with brain disease was high

and the number of patients increases year after year. This has also, to some degree, increased the workload of medical staff in this field. A reliable and effective method of identifying bone lesions in brain tumor images that has addressed the rising demand is urgently needed. This work investigated the possibility of removing the CT simulator and replacing it with pseudo-CT for the identification of bone lesions. In order to improve accuracy and to achieve pCT image generation without manual intervention, this article proposes deep convolutional models with this in mind. The model is primarily made up of CNN and an integrated GAN. The superiority and efficacy of the proposed model was demonstrated by the implementation of the simulation. Clinical assessment indicates that there is potential for clinical use of the proposed method and may contribute to widespread use of other modalities of imaging. In addition, the structure suggested is versatile and can be applied to other applications.

REFERENCES

[1] Largent, Axel, Louis Marage, Ivan Gicquiau, J-C. Nunes, Nick Reynaert, Joël Castelli, Enrique Chajon et al. 2020.Head-and-Neck MRI-only radiotherapy treatment planning: From acquisition in treatment position to pseudo-CT generation. Cancer/Radiothérapie 24, no. 4 : 288-297.

[2] Fei, B., Yang, X., Nye, J.A., Aarsvold, J.N., Raghunath, N., Cervo, M., Stark, R., Meltzer, C.C., Votaw, J.R.: MR/PET quantification tools: registration, segmentation, classification, and MR-based attenuation correction. Med. Phys. 39(10), 6443–6454.

[3] Rundo, L., Militello, C., Tangherloni, A., Russo, G., Vitabile, S., Gilardi, M.C., Mauri, G.2018. NeXt for neuro-radiosurgery: a fully automatic approach for necrosis extraction in brain tumour MRI using an unsupervised machine learning technique. Int. J. Imaging Syst. Technol. 28(1), 21–37

[4] Gunawardena, K., Rajapakse, R., Kodikara, N.: Applying convolutional neural networks for pre-detection of Alzheimer's disease from structural MRI data.2017.In: 2017 24th International Conference on Mechatronics and Machine Vision in Practice (M2VIP), pp. 1–7. IEEE

[5] Valverde, S., Cabezas, M., Roura, E., Gonz´alez-Vill`a, S., Pareto, D., Vilanova, J.C., Ramio-Torrenta, L., Rovira, A., Oliver, A., Llad o, X.2017. Improving automated multiple sclerosis lesion segmentation with a cascaded 3D convolutional neural network approach. NeuroImage 155, 159–168

[6] Praveen, G., Agrawal, A., Sundaram, P., Sardesai, S.2018. Ischemic stroke lesion segmentation using stacked sparse autoencoder. Comput. Biol. Med.

[7] Edmund, Jens M., and Tufve Nyholm. 2017.A review of substitute CT generation for MRI-only radiation therapy. Radiation Oncology 12, no. 1 : 1-15.

[8] Maspero, Matteo, Cornelis AT Van den Berg, Guillaume Landry, Claus Belka, Katia Parodi, Peter R. Seevinck, Bas W. Raaymakers, and Christopher Kurz. 2017.Feasibility of MR-only proton dose calculations for prostate cancer radiotherapy using a commercial pseudo-CT generation method." Physics in Medicine & Biology 62, no. 24 : 9159.

[9] Wang, Tonghe, Nivedh Manohar, Yang Lei, Anees Dhabaan, Hui-Kuo Shu, Tian Liu, Walter J. Curran, and Xiaofeng Yang. 2019.MRI-based treatment planning for brain stereotactic radiosurgery: dosimetric validation of a learning-based pseudo-CT generation method." Medical Dosimetry 44, no. 3 : 199-204.

[10] Lei, Yang, Tonghe Wang, Joseph Harms, Ghazal Shafai-Erfani, Sibo Tian, Kristin Higgins, Hui-Kuo Shu et al.2019.MRI-based pseudo CT generation using classification and regression random forest." In Medical Imaging : Physics of Medical Imaging, vol. 10948, pp. 996-1001. SPIE

[11] Arabi, Hossein, and Habib Zaidi. 2016.One registration multi-atlas-based pseudo-CT generation for attenuation correction in PET/MRI. European journal of nuclear medicine and molecular imaging 43, no. 11 : 2021-2035.

[12] Korsholm, Marie E., Line W. Waring, and Jens M. Edmund.2014.A criterion for the reliable use of MRI-only radiotherapy." Radiation Oncology 9, no. 1 : 1-7.

[13] Stanescu, T., H. S. Jans, N. Pervez, P. Stavrev, and B. G. Fallone.2008.A study on the magnetic resonance imaging (MRI)-based radiation treatment planning of intracranial lesions. Physics in Medicine & Biology 53, no. 13 : 3579.

[14] Kemppainen, Reko, Sami Suilamo, Terhi Tuokkola, Paula Lindholm, Martin H. Deppe, and Jani Keyriläinen.2017.Magnetic resonance-only simulation and dose calculation in external beam radiation therapy: a feasibility study for pelvic cancers. Acta Oncologica 56, no. 6 : 792-798.

[15] Sjölund, Jens, Daniel Forsberg, Mats Andersson, and Hans Knutsson.2015.Generating patient specific pseudo-CT of the head from MR using atlas-based regression." Physics in Medicine & Biology 60, no. 2 : 825.

[16] Greer, Peter, Jarad Martin, Mark Sidhom, Perry Hunter, Peter Pichler, Jae Hyuk Choi, Leah Best et al. 2019.A multi-center prospective study for implementation of an MRI-only prostate treatment planning workflow. Frontiers in oncology 9 : 826.

[17] Oktay, Ozan, Jay Nanavati, Anton Schwaighofer, David Carter, Melissa Bristow, Ryutaro Tanno, Rajesh Jena et al. 2020.Evaluation of deep learning to augment image-guided radiotherapy for head and neck and prostate cancers." JAMA network open 3, no. 11 : e2027426-e2027426.

[18] Shafai-Erfani, Ghazal, Tonghe Wang, Yang Lei, Sibo Tian, Pretesh Patel, Ashesh B. Jani, Walter J. Curran, Tian Liu, and Xiaofeng Yang. 2019.Dose evaluation of MRI-based synthetic CT generated using a machine learning method for prostate cancer radiotherapy. Medical Dosimetry 44, no. 4 : e64-e70

[19] Hemsley, Matt, Brige Chugh, Mark Ruschin, Young Lee, Chia-Lin Tseng, Greg Stanisz, and Angus Lau.2020. Deep Generative Model for Synthetic-CT Generation with Uncertainty Predictions. In International Conference on Medical Image Computing and Computer-Assisted Intervention, pp. 834-844. Springer, Cham,

[20] Andres, Emilie Alvarez, Lucas Fidon, Maria Vakalopoulou, Marvin Lerousseau, Alexandre Carré, Roger Sun, Guillaume Klausner et al. 2020.Dosimetry-driven quality measure of brain pseudo computed tomography generated from deep learning for MRI-only radiation therapy treatment planning.International Journal of Radiation Oncology* Biology* Physics 108, no. 3 : 813-823.

[21] Torrado-Carvajal, Angel, Javier Vera-Olmos, David Izquierdo-Garcia, Onofrio A. Catalano, Manuel A. Morales, Justin Margolin, Andrea Soricelli, Marco Salvatore, Norberto Malpica, and Ciprian Catana. 2019.Dixon-VIBE deep learning (DIVIDE) pseudo-CT synthesis for pelvis PET/MR attenuation correction." Journal of nuclear medicine 60, no. 3 : 429-435.

[22] Largent, Axel, Anaïs Barateau, Jean-Claude Nunes, Eugenia Mylona, Joël Castelli, Caroline Lafond, Peter B. Greer et al.2019.Comparison of deep learning-based and patch-based methods for pseudo-CT generation in MRI-based prostate dose planning." International Journal of Radiation Oncology* Biology* Physics 105, no. 5 : 1137-1150.

[23] Open Access Series of Imaging Studies. OASIS Database. 2007. URL: http://www.oasisbrains.org (visited on 09/13/2018).

[24] Ranganathan, G.2021. A study to find facts behind preprocessing on deep learning algorithms. Journal of Innovative Image Processing (JIIP) 3, no. 01 : 66-74.

[25] Ranjan, Kumar G., Debesh S. Tripathy, B. Rajanarayan Prusty, and Debashisha Jena.2021. An improved sliding window prediction-based outlier detection and correction for volatile time-series. International Journal of Numerical Modelling: Electronic Networks, Devices and Fields 34, no. 1: e2816.

[26] Yan, Yujia, Guangxin Wu, Yang Dong, and Yechao Bai.2021. An Improved MSR-Based Data-Driven Detection Method Using Smoothing Pre-Processing. IEEE Signal Processing Letters 28 : 444-448.

[27] Cieslak, Matthew, Philip A. Cook, Xiaosong He, Fang-Cheng Yeh, Thijs Dhollander, Azeez Adebimpe, Geoffrey K. Aguirre et al.2021. QSIPrep: an integrative platform for preprocessing and reconstructing diffusion MRI data.Nature methods 18, no. 7 : 775-778.

[28] Nahiduzzaman, Md, Md Omaer Faruq Goni, Md Shamim Anower, Md Robiul Islam, Mominul Ahsan, Julfikar Haider, Saravanakumar Gurusamy, Rakibul Hassan, and Md Rakibul Islam.2021. A Novel Method for Multivariant Pneumonia Classification Based on Hybrid CNN-PCA Based Feature Extraction Using Extreme Learning Machine With CXR Images. IEEE Access 9 : 147512-147526.

[29] Şahin, Durmuş Özkan, Oğuz Emre Kural, Sedat Akleylek, and Erdal Kılıç. 2021.A novel permission-based Android malware detection system using feature selection based on linear regression.Neural Computing and Applications : 1-16.

[30] Cao, Hu, Yueyue Wang, Joy Chen, Dongsheng Jiang, Xiaopeng Zhang, Qi Tian, and Manning Wang.2021. Swin-unet: Unet-like pure transformer for medical image segmentation. arXiv preprint arXiv:2105.05537.

[31] Kumar, Krishanth, V. Sowmya, E. A. Gopalakrishnan, and K. P. Soman. 2022 Classification of Class-Imbalanced Diabetic Retinopathy Images Using the Synthetic Data Creation by Generative Models.In Intelligent Sustainable Systems, pp. 15-24. Springer, Singapore.

[32] Andreini, Paolo, Giorgio Ciano, Simone Bonechi, Caterina Graziani, Veronica Lachi, Alessandro Mecocci, Andrea Sodi, Franco Scarselli, and Monica Bianchini.2022. A Two-Stage GAN for High-Resolution Retinal Image Generation and Segmentation.Electronics 11, no. 1 : 60.